

A&A manuscript no.
(will be inserted by hand later)

Your thesaurus codes are:
06 (08.22.3; 03.13.2; 08.16.4; 03.20.4; 11.13.1; 08.05.3)

ASTRONOMY
AND
ASTROPHYSICS

AGAPEROS: Searching for variable stars in the LMC Bar with the Pixel Method^{*}

I. Detection, astrometry and cross-identification^{**}

A.-L. Melchior^{1,2}, S.M.G. Hughes³, and J. Guibert⁴

¹ Astronomy Unit, Queen Mary and Westfield College, Mile End Road, London E1 4NS, UK

² DEMIRM (UMR 8540), Observatoire de Paris, 61, Avenue de l'Observatoire, 75 014 Paris Cedex, France

³ Institute of Astronomy, University of Cambridge, Madingley Road, Cambridge CB3 0EZ, UK

⁴ Centre d'Analyse des Images de l'INSU (UMR 8633), Observatoire de Paris, 61 avenue de l'Observatoire, 75 014 Paris, France

Received / Accepted

Abstract. We extend the work developed in previous papers on microlensing with a selection of variable stars. We use the Pixel Method to select variable stars on a set of 2.5×10^6 pixel light curves in the LMC Bar presented elsewhere. The previous treatment was done in order to optimise the detection of long timescale variations (larger than a few days) and we further optimise our analysis for the selection of Long Timescale and Long Period Variables (LT&LPV). We choose to perform a selection of variable objects as comprehensive as possible, independent of periodicity and of their position on the colour magnitude diagram. We detail the different thresholds successively applied to the light curves, which allow to produce a catalogue of 632 variable objects. We present a table with the coordinate of each variable, its EROS magnitudes at one epoch and an indicator of blending in both colours, together with a finding chart.

A cross-correlation with various catalogues shows that 90% of those variable objects were undetected before, thus enlarging the sample of LT&LPV previously known in this area by a factor of 10. Due to the limitations of both the Pixel Method and the data set, additional data – namely a longer baseline and near infrared photometry – are required to further characterise these variable stars, as will be addressed in subsequent papers.

Key words: Stars: variables: general – Methods: data analysis – AGB and post-AGB – Techniques: photometric – Galaxies: Magellanic Clouds – Stars: evolution

1. Introduction

The microlensing searches, motivated by the study of dark matter in galaxies and its possible fraction of compact objects (hereafter Machos), have collected some unprecedented databases of images of neighbouring galaxies, and in particular of the Large Magellanic Cloud (LMC). The microlensing candidates are compatible with large Macho masses, and exhibit long timescale variations, typically 10-200 days (Alcock et al. 1997abc, Renault et al. 1997, Palanque-Delabrouille et al. 1998, Alard et al. 1997, Udalski et al 1994, Ansari et al. 1999). Possible contamination by variable stars is often suggested (e.g. della Valle & Livio 1996), but no systematic searches for variable objects have been undertaken so far on the microlensing databases. Whereas particular variables, such as RR Lyrae and cepheids are relatively well understood, little statistical information is known about the Long Timescale and Long Period Variable stars (hereafter LT&LPV), with timescales/periods in the range of ~ 100 to ~ 800 days, which are an important stage of stellar evolution. They are easily rejected for these microlensing searches either with a cut on marginal stellar populations identified on the colour magnitude diagram (hereafter CMD) or by their periodicity. Aperiodic signals which do not satisfy these simple criteria are however more difficult to discriminate and to select.

In this paper, we perform a selection of variable objects on pixel light curves covering a 0.25 deg^2 field of the LMC Bar. We used the pixel light curves produced in Melchior et al (1999, hereafter paper I) adopting looser thresholds than those used for the selection of microlensing events in Melchior et al. (1998, hereafter paper II). In Sect. 2, we summarise the characteristics of the data set. In Sect. 3, we discuss the automatic selection procedure used to keep all significant genuine variable stars. In Sect. 4, we introduce a magnitude estimate for each variable and display its position in the colour-magnitude diagram. In Sect. 5,

Send offprint requests to: Anne-Laure Melchior

^{*} This work is based on data collected by the EROS collaboration.

^{**} Tables 2 is also available in electronic form at the CDS via anonymous ftp to cdsarc.u-strasbg.fr (130.79.128.5) or via <http://cdsweb.u-strasbg.fr/Abstract.html>

Correspondence to: A.L.Melchior@obspm.fr

we describe the procedure used to obtain the equatorial coordinates. In Sect. 6, we cross-identify the selected variable stars with existing databases. Finally, we provide the catalogue in Sect. 7.

2. EROS CCD data and AGAPEROS pixel light curves

2.1. EROS CCD data

We use the EROS-1 CCD dataset, taken at ESO over the period 1991 December 18 to 1992 April 11, using a 40 cm telescope with a wide field camera composed of 16 CCD chips, each with 400×579 pixels of 1.21 arcsec (Arnaud et al., 1994b, Queinnec, 1994, Aubourg et al., 1995 and Grison et al., 1995). Images of one field in the LMC Bar were taken in two wide non-standard blue ($\bar{\lambda} = 490$ nm) and red ($\bar{\lambda} = 670$ nm) filters, with a mean seeing of 2. arcsec.

The EROS-1 experiment (Arnaud et al. 1994a,b) was motivated by the study of dark compact objects in the dark halo of our Galaxy and contributed to show that the so-called brown dwarves could not be a significant component of the dark matter (Renault et al. 1997).

This dataset, treated in Paper I, is composed of some 1 000 images per CCD and per colour spread over 120 days. Only 10 CCD fields were available in 91-92, so we restrict our analysis to this field of 0.25 deg^2 .

2.2. AGAPEROS pixel light curves

For this selection, we use the pixel light curves produced in Paper I, as a first application to the EROS data of the Pixel Method (Baillon et al. 1993). In Paper I, we described in detail the data treatment we applied to the EROS-1 data set described in the previous paragraph. The frames were first geometrically and photometrically aligned with respect to a reference image. In order to decrease the level of noise on these 8-12 min exposures, we averaged the 10-20 frames available each night. Whereas this increases our sensitivity to possibly dim LT&LPV, *this is not optimised for the detection of short period variable stars, already studied elsewhere on the same data set (Grison et al 1995, Beaulieu et al. 1995, Hill & Beaulieu 1997)*.

The data are then arranged in super-pixel light curves, and an empiric seeing correction is then applied to each light curve. The limitations of this technique reside in the conversion of pixel fluxes in magnitudes, which can be done efficiently with kernel convolution techniques developed by Tomaney & Crotts (1996) and Alard (1998). Due the large filters of the EROS database and the short baseline (120 days) available with this data set, we choose to postpone this step to the next paper, which will produce periods with 3-years light curves together with a cross-identification with the DENIS photometry. In this paper, we provide a magnitude estimate for one epoch, together

Table 1. Selection procedure. Column (A) gives the parameters used for thresholding, (B) gives the value of the threshold. (C) provides the number of light curves kept at each step. Numbers surrounded by boxes provide the actual threshold used and the actual number of curves selected. Other numbers show how the weakening or strengthening of these thresholds affect the number of selected light curves. This procedure is further illustrated in Fig. 1.

Step	Parameters (A)	Threshold (B)	Number (C)
(0)	Starting point after	excision	2 093 584 (100 %)
(1)	$\text{Min}((\frac{\sigma_1}{\sigma_2}) _B, (\frac{\sigma_1}{\sigma_2}) _R)$	< 0.7	133 394 (6.37 %)
		< 0.6	32 067 (1.53 %)
		< 0.5	11 369 (0.54 %)
(2)	$\text{Max}(L_B, L_R)$	> 300	24 892 (1.19 %)
		> 400	20 942 (1.00 %)
		> 500	17 857 (0.85 %)
(3)	Clusters identification		3 782 (0.18 %)
(4)	$\text{Max}(L_B, L_R)$ $\text{Min}((\frac{\sigma_1}{\sigma_2}) _B, (\frac{\sigma_1}{\sigma_2}) _R)$	> 400	3 637 (0.17 %)
		< 0.6	3 381 (0.16 %)
(5)	N_{clus}	> 4	999 (0.05 %)
		> 6	747 (0.04 %)
		> 10	544 (0.03 %)

with an indication of blending, and put the emphasis on the selection procedure and the cross-identification with other catalogues.

The light curves we use in the following to select variable stars correspond to the super-pixel flux $\phi_n(t)$ measured at different epochs n :

$$\phi_n(t) = \phi_{star}(t) + \phi_{sky} \quad (1)$$

where ϕ_{sky} includes the sky and stellar background, and $\phi_{star}(t)$ is the flux of the variable star.

3. Selection of genuine variable stars

We apply an automatic selection of genuine luminosity variations to the 91-92 dataset. Firstly, we introduce the definition of a variation. Secondly, we adjust the thresholds in order to keep genuine variations but reject most artifacts due to noise. Last, we carefully inspect selected light curves close to bad pixels.

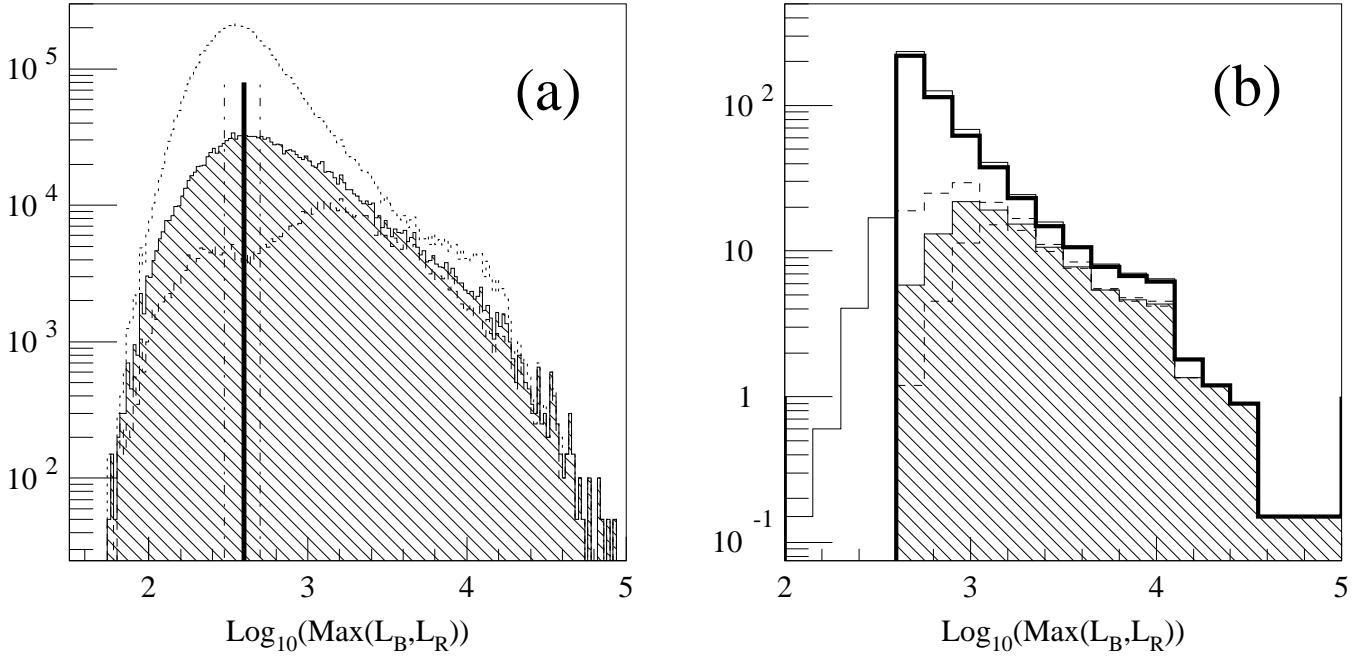


Fig. 1. Effect of the selection procedure on the $\text{Max}(L_B, L_R)$ distribution. Panel **a)** illustrates the effect of the steps (1) and (2) of the selection procedure indicated in Tab. 1. The hatched area corresponds to the pixels kept at step (1). The dashed and dotted histograms each show how this distribution is affected if this threshold is changed as indicated in Tab. 1. The thick line displays the effect of step (2). The dot-dashed lines correspond to the weakening/strengthening of this cut. Panel **b)** illustrates the effects of steps (4) and (5). The large amplitude histogram shows the distribution after step (3), the thick-line histogram shows the result of step (4), and the hatched area corresponds to pixels kept at the end of step (5). The dashed histograms show the sensitivity of this last threshold.

3.1. Definition of a variation

A baseline flux (ϕ_{bl}) is calculated for each super-pixel light curve by sorting all points in order of increasing flux, with ϕ_{bl} being the 10th sorted point. σ_{bl} is the error associated with the baseline flux determination. For a sample taken from a Gaussian distribution with a standard deviation σ this estimate lies 1.3σ below the mean value of the distribution.

Deviations from this baseline are recorded when measurements lie $3\sigma_n$ above the baseline:

$$\sigma_n = \sqrt{\sigma_n'^2 + \sigma_{bl}^2} \quad (2)$$

where σ_n' is the error associated with each super-pixel flux computed in Paper I for night n . These deviations are quantified in each colour with a likelihood function (L):

$$L = -\ln \left(\prod_{n \in \text{bump}} P(\phi \geq \phi_n) \text{ given } \begin{cases} \phi_{bl} \\ \sigma_n \end{cases} \right) \quad (3)$$

where ϕ_n is the super-pixel flux for the measurement n . All the measurements above ϕ_{bl} are accounted for.

3.2. Minimal threshold

With the definition introduced above, we apply the selection procedure summarised in Tab. 1.

First of all we excise the pixels, covering 3.4% of the CCD fields, which exhibit obvious spurious variations (such as bad columns). In addition, in order to remove automatically artifacts due to bad pixels, we remove from the light curves the epochs for which there is at least one pixel which datum is at zero within a 11×11 window centred on the super-pixel. (1) We require a regularity condition to remove the noise: the ratio σ_1/σ_2 has to be smaller than 0.6 in at least one colour, with:

$$\sigma_1^2 = \frac{2}{3(N-2)} \sum_{n=2}^{N-1} \left[\frac{\phi_{n+1} - \phi_{n-1}}{2} - \phi_n \right]^2 \quad (4)$$

$$\sigma_2^2 = \frac{1}{(N-1)} \sum_{n=1}^N [\phi_n - \phi_{mean}]^2 \quad (5)$$

where ϕ_{mean} is the mean super-pixel flux and N is the total number of measurements on each light curve. (2) We then select the light curves which vary such that $L > 400$ in at least one colour. As there are as many super-pixels as pixels, a genuine variable is expected to affect all the

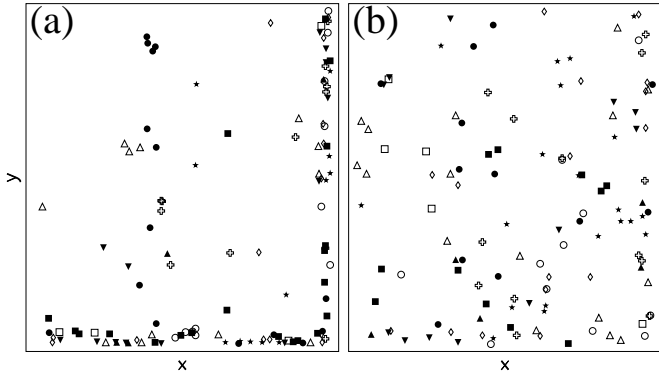


Fig. 2. Artifact removals. Panel a) displays the positions of the 116 rejected light curves on the CCD chips. Panel b) shows a similar distribution but for those among the 237 light curves close to CCD defects that have been kept. Each symbol corresponds to a different chip. Each panel corresponds to the size of the chips $x \in [0, 400]$, $y \in [0, 579]$.

super-pixels within the seeing spot. (3) We search for clusters of super-pixels (using a Friend of Friends algorithm), and keep the central pixel of the clusters if (4) the previous requirements are also satisfied for these pixels and, if (5) the number N_{clus} of super-pixels that compose each cluster is larger than 6. These requirements eliminate most artifacts due to bright stars¹ and CCD defects that do not exhibit a clear spatial PSF-like pattern. We finally keep 747 super-pixel light curves. The sensitivity of these thresholds is illustrated in Fig. 1. Among the 747 selected variations, two have been counted twice², leaving 745 independent light curves.

3.3. Artifact removals

We select 237 light curves for which there is at least one bad pixel (saturated or set at zero) within a 21×21 window centred on the selected pixel for at least one epoch and at least one colour. A careful visual inspection of these light curves shows 121 genuine variable stars against 116 artifacts, subsequently removed. Figure 2 shows that the removed light curves are mainly concentrated close to the edges, whereas the distribution of the kept light curves (among the 237) is more uniform. We finally end with a catalogue of 631 variable stars.

4. Magnitude estimation

Whereas the pixel method of analysis is able to detect variable stars beyond the crowding limit, it does not measure photometry – total flux – of these objects, that can

¹ Super-pixels around a few bright stars exhibit artifacts such that the spatial correlation of the position of these super-pixels looks like a partial ring or an arc.

² For computing reasons, each chip has been cut into two pieces with an overlapping region through the analysis.

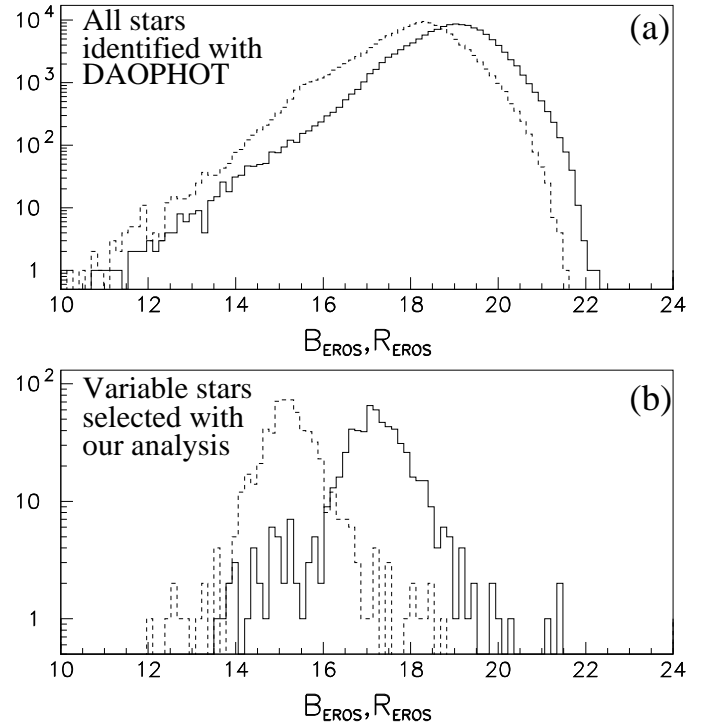


Fig. 3. Luminosity functions in blue (full line) and in red (dashed line) at the epoch $JD=2448678.3$. The upper histograms a) correspond to the magnitudes estimated for all the stars with DAOPHOT. The lower histograms b) correspond to the magnitudes estimated as described in Sect. 4.1 for the selected variable stars.

be blended or even unresolved on part of the light curves. Obtaining their photometry would give a first indication of the type of the variable stars. Hence in this section, we associate a magnitude and colour to each flux measurement.

4.1. Pseudo-aperture photometry

As discussed in Paper II, the flux of the super-pixel is composed of the fraction of the flux of the star plus the local background (from sky and undetected stars). For our sample of variable stars, we can presume that there is a star within the corresponding super-pixel and that its flux significantly contributes to this super-pixel, at least at the maximum of the variation. Because of the crowding conditions, standard background estimates (circular annulus for example, see Stetson (1987)) fail and cannot be used in an automatic way. Hence, we choose to perform a pseudo-aperture photometry as follows. For an image taken in the middle of the period of observation ($JD2448678.3$) and with an average seeing, we use the PSF fitting procedure of DAOPHOT (Stetson, 1987) to measure the fluxes of the resolved stars, and the background below them. This thus gives a local estimate of the background that is the less affected by the crowding of the field. Then for each

selected super-pixel we look for the detected star that is closest. The background estimate associated with this star is supposed to be the same as the one present below the variable star (and is even identical if the variable stars are resolved on this reference frame). This background is subtracted from the super-pixel flux. This flux is then corrected for the seeing fraction and converted into a magnitude, corresponding to an isolated star.

Whereas this definition of the sky-background is rather robust to the crowding conditions, the magnitude estimation is not necessary so, as some additional flux (stellar background) could contribute to the super-pixel due to neighbours. We thus quantify the blending with the ratio ϕ_c/ϕ_0 computed as follows: the flux ϕ_c is the averaged value computed along the light curve of the central pixel of the super-pixel, and the flux ϕ_0 is a similar average of the 8 surrounding pixels within the super-pixel. The behaviour of this parameter is described in the Appendix.

Optimised star detection with DAOPHOT allows to detect 135 098 stars in blue and 142 870 stars in red. The corresponding luminosity function computed with DAOPHOT for all the stars present on the studied field, exhibited in Fig. 3a, shows that the star detection is in first approximation complete down to magnitude 18 in red and 19 in blue. Figure 3b shows that the magnitude distributions at the same epoch for the selected variable stars peak at the bright end, whereas the stars are redder than average with $B_{EROS} - R_{EROS} \simeq 2$. Whereas it is difficult to compute our detection efficiencies as no reliable theoretical distribution of variable stars is available, it is clear that we do not detect a population of variable stars unresolved at minimum, even though we do detect a tail of this distribution with very dim stars in at least one colour.

4.2. Colour-magnitude diagram

Figure 4 displays the position of the 631 variable stars in the CMD. This CMD has been obtained with the resolved stars detected with DAOPHOT in both colours. The conversion of the EROS magnitudes into a standard system has been studied by Grison et al. (1995), but introduces significant systematic errors especially for stars with $B_{EROS} - R_{EROS} > 1$. We hence choose to work in the EROS system. The crowding limit prevents the detection of stars with $R_{EROS} > 19$. The main sequence and red clump are clearly identified. Very little variations of the CMD are observed from one chip to another suggesting a uniform stellar population across this field. The vast majority of the detected variable stars lies in the red part. A visual inspection of the corresponding light curves shows that they are compatible with LT&LPV. This catalogue offers the perspective to systematically study the later stages of stellar evolution within the LMC Bar. However, the isochrones superimposed on Fig. 4 illustrate the difficulty to classify variable stars with the sole CMD, as it is impossible to disentangle their age and mass for a given

metallicity. The photometric system made it also inappropriate for further interpretation with this sole data. Due to their complexity and the difficulties to model them, the LT&LPV are better characterised in the IR, as addressed in a subsequent paper. Some “bluer” objects have also been detected and they will be classified when we study their periodicity.

As shown in Fig. 4, variable stars not significantly affected by crowding ($\phi_c/\phi_0 > 3$) lie in areas of the colour-magnitude diagram corresponding to stars expected variable. Those affected by blending and crowding will have to be treated with caution. In the CMD areas where the larger number of LT&LPV have been detected, in the magnitude ($R_{EROS} = 14.6 - 15.8$) and colour ($B_{EROS} - R_{EROS} = 1.7 - 2.3$) ranges, about 17% of the stars exhibit a variation detected with our analysis.

It is also clear that the vast majority of the detected variable stars are above the crowding limit. The few outliers that can be noticed correspond to stars unresolved in at least one colour, but their number does not exceed 5 % of the total. In terms of microlensing, this means that events due to unresolved stars in the LMC will not be significantly contaminated by the bulk of variable stars. In further galaxies, like M31, variable stars will be a more troublesome affair, and will have to be carefully studied (e.g. Crots & Tomaney 1996). However, high amplification microlensing events are far less likely to be mimicked by an intrinsic variation (Ansari et al. 1999), and will allow to probe possible biases introduced by variable stars.

5. Astrometric reduction

The rectangular sky area covered by the EROS-1 chips is enclosed in a circle of radius $\sim 30'$ centred on the position $\alpha = 05^h 21^m 52.1^s$; $\delta = -69^\circ 34' 16''$ (2000.0). In this region, the density of PMM astrometric standards³ is highly irregular, e.g. four $\sim 20' \times 15'$ areas are completely empty. This is mainly due to the crowding of the survey plates used at USNO. We therefore chose to use a U plate taken at the ESO 1m Schmidt telescope to define the secondary astrometric standards. This plate was scanned with the MAMA microdensitometer⁴, and reduced to the International Celestial Reference System (ICRS)⁵ with the ACT catalogue⁶. Thanks to the modest sensitivity of the U emulsion/filter combination, the effects of crowding are reduced. A remarkably regular distribution of stars is detected with the SExtractor software (Bertin & Arnouts, 1996), with on average 2 700 stars per chip.

The secondary standards ($\sim 1500/\text{chip}$) are identified to EROS stars using a first linear transformation based

³ <http://ftp.nofs.navy.mil/projects/pmm/>

⁴ MAMA (<http://dsmama.obspm.fr>) is operated by INSU (Institut National des Sciences de l'Univers) and Observatoire de Paris.

⁵ <http://hpiers.obspm.fr/webiers/general/syframes/SY.html>

⁶ <http://vizier.u-strasbg.fr/cgi-bin/VizieR?-source=I/246>

on some 15 visually cross-identified stars per chip. The astrometric reduction software (Robichon et al. 1995) is then run using this set of references. After iteration, the final 2nd order reduction keeps 1000 stars per chip with final rms deviation of the order of 0.2".

According to the galactic model⁷ from Besançon, more than 95% of the secondary references belong to LMC. Furthermore, we check that the global proper motion of the LMC (Kroupa & Bastian, 1997), together with upper limits on its internal velocity dispersion cannot affect the positions of our standards by more than 30 mas, over the 848-days separating the ESO plate from the EROS reference.

6. Cross-identifications

The detected variable stars are uniformly distributed along the CCD chips, and no obvious bias (due e.g. to internal extinction) are suspected. In order to appreciate the sensitivity of our analysis, we cross-identified this catalogue with previous works. Among the 631 variable stars presented here, 72 have already been studied elsewhere. We considered the main catalogues which covered this area, namely the catalogues of LT&LPV by Hughes (1989), eclipsing binaries and cepheids by EROS (Grison et al., 1994 and Beaulieu et al. 1996), radio sources (Marx et al., 1999), X-ray sources (Haberl & Pietsch, 1999), as well as the General Catalogue of Variable Stars⁸ (Artiukhina et al., 1995) and the NED⁹ data-base. We define a genuine cross-identification any object whose offsets with respect to the variable objects detected here are smaller than $\Delta\alpha_{\max} = 5''$ and $\Delta\delta_{\max} = 5''$.

Among the 58 LT&LPV found by Hughes (1989) in this field, 41 have been detected here, 12 are missed due to CCD defects (one of those is rejected with the visual inspection described in Sect. 3.3). This gives the order of magnitude of the completeness of our sample over a 120-day window: we typically miss up to 20% of genuine variable stars due to CCD defects. More interestingly, the last 5 missing LT&LPV escape our selection for no obvious reason. One of them (SHV0527122-695006) has been subsequently observed in the near-infrared (Hughes & Wood 1990): it did not follow the $(K, \log P)$ relation, and was interpreted as a supergiant or a foreground Mira. According to the DAOPHOT magnitudes measured at epoch $JD=2448678.3$ $B_{\text{EROS}} = 15.7$ and $R_{\text{EROS}} = 13.7$, it is consistent with a supergiant. The 4 remaining, namely SHV0516251-693241, SHV0519415-693441, SHV0522220-

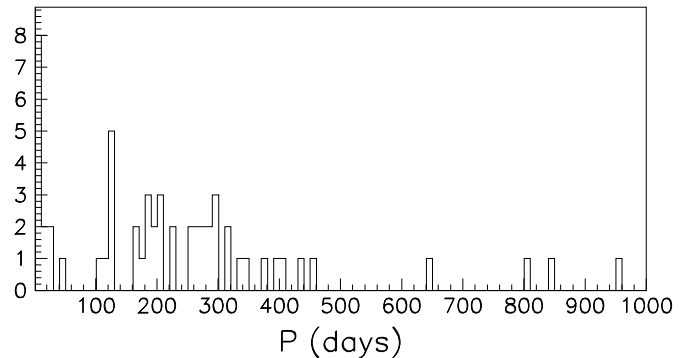


Fig. 5. Histogram of the periods. We present here the periods measured elsewhere which correspond to 57 of the 631 variable stars detected here.

694441, SHV0522251-692902 – not observed subsequently by Hughes & Wood (1990) – were reported by Hughes (1989) with a low amplitude ($\Delta I \simeq 0.5$ mag.) and 3 of them were only marginally periodic. Moreover, our non-detection can be explained for some of them by changes in mass-loss rates as suggested by Whitelock (1997). The extension of this work with a longer baseline together with DENIS photometry is expected to provide further arguments about this kind of behaviour (in preparation).

The short periodic variable stars from the EROS catalogue (Grison et al., 1994, and Beaulieu et al., 1996) are missed here for most of them: short timescale variations are broken by the averaging procedure as explained in Sect. 2. Only 22 out of the 181 variable stars previously detected by EROS are present in this catalogue. In addition, 5 of the 7 pre-main-sequence candidates published by Beaulieu et al. (1996) have been detected. None of the radio-sources, detected by Marx et al. (1997), are lying in the studied field. 2 X-ray sources detected with ROSAT (Haberl & Pietsch, 1999) are present in the field, but none of our variable stars lies in the 90%CL error box of those sources. 29 extragalactic sources (but not necessarily variable) from NED are present in the field, none is among the variable stars detected here. Last, whereas 129 sources from the GCVS are lying in the field, 52 are selected here. Most of them were also in the catalogues mentioned above. According to the GCVS classification, among these 52 variables, 17 are Miras, 26 semi-regulars, 2 irregulars, and 7 cepheids.

A total of 72 sources out of 631 were previously reported, 57 of which have a published period. Those are presented in Fig. 5: they are clearly of the order of 100-300 days. A visual inspection confirms that besides a few short periods, these timescales are quite representative of the bulk of a distribution dominated by LT&LPV.

7. Catalogue

LT&LPV (“Red” variable stars) represent the bulk of the stars presented in this catalogue. Figures 6 and 7 show

⁷ <http://WWW.obs-besancon.fr/www/modele/s-tab.html>

⁸ We used the electronic version of the GCVS (<http://www.sai.msu.su/groups/cluster/gcvs/gcvs/>), supported by the Russian Foundation for Basic Research.

⁹ The NASA/IPAC Extragalactic Database (NED) is operated by the Jet Propulsion Laboratory, California Institute of Technology, under contract with the National Aeronautics and Space Administration.

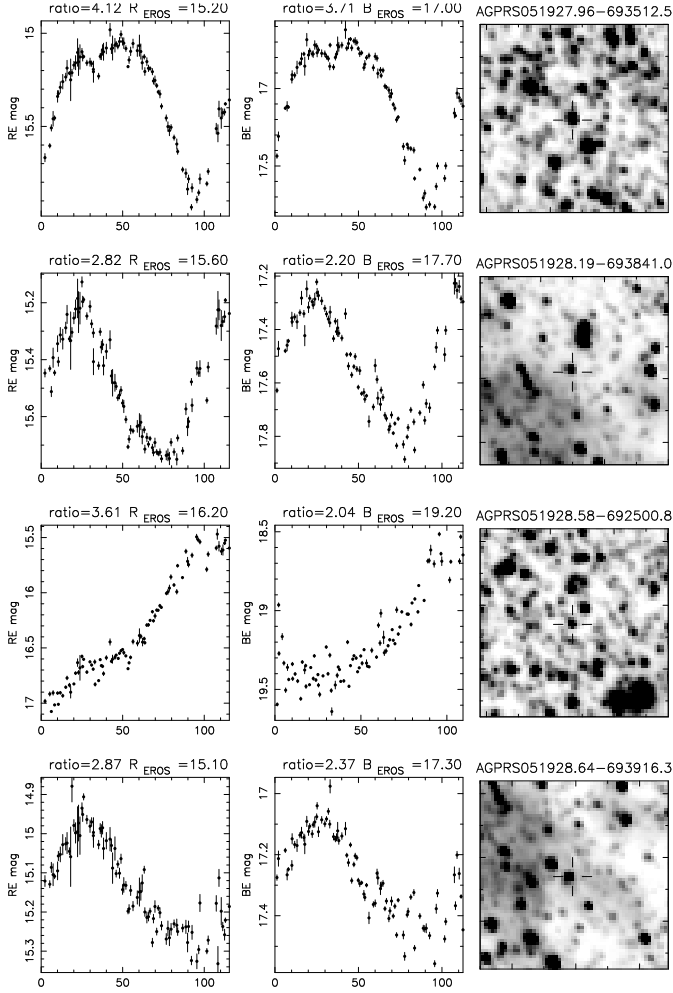


Fig. 6. Examples of red variables. The light curves in red and blue together with the corresponding finding chart in red are displayed for 4 red variable stars from the catalogue. The ϕ_c/ϕ_0 ratio is provided for each light curve, as well as the magnitude at JD=2448678.3. Note the fact that the large dispersion with respect to the errors observed for some blue light curves is due to blending and those light curves have a low ϕ_c/ϕ_0 ratio.

typical light curves detected with the corresponding finding charts. Amplitudes measured over 120 days can be as low as 0.1 mag up to several magnitudes, depending on the timescale, and brightness range. The limitations (in the photometry) due to the crowding are also illustrated. The error bars (estimated in Paper I) account for the level of photon noise and other residual errors, but they do not account for the effect of crowding on the star flux. For light curves with $\phi_c/\phi_0 \leq 3$, error bars are underestimated with respect to the scatter along the variation. This explains why the amplitude of variations in blue can be smaller (or comparable) than in red for a few LT&LPV: the crowding is more important in blue and larger amplitudes of variation are expected on dimmer stars. Hence, we do not attempt to extract information about the amplitude, but

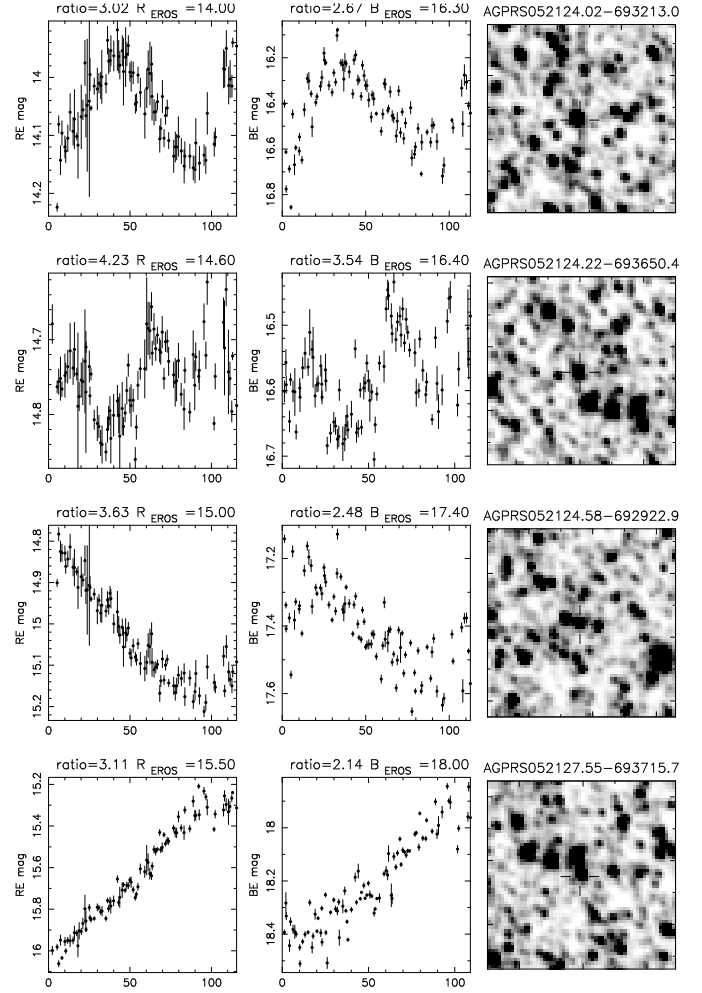


Fig. 7. Examples of red variables. Same as Fig. 6.

provide magnitude estimates at one epoch with the ϕ_c/ϕ_0 ratio. For most of them, the timescale of the variation is much longer than the period of observation, and the periodicity will not be studied here.

Table 2 contains the following informations. *Column 1:* The position, at J2000.0 epoch, is incorporated into the name of each variable, in accordance with IAU convention (Dickel et al. 1987); *Column 2:* N/X/Y: chip number N and position (X,Y) on the chip. There were 10 chips on the EROS-1 CCD camera. *Column 3:* the ϕ_c/ϕ_0 ratio in blue and red; *Column 4:* the B_{EROS} and R_{EROS} magnitude estimate at epoch JD=2448678.3; *Column 5:* the number of stars detected by DAO in the super-pixel at epoch JD=2448678.3 in B/R; *Column 6 and 7:* the B_{EROS} and R_{EROS} magnitudes (at the same epoch) of the closest stars as estimated by DAOPHOT. Figures in bracket (on a second line) provide the magnitude of another star detected in the super-pixel. *Column 8:* identification with the other databases, discussed in the text. The Harvard variable numbers are given, as well as variables (WBP) detected by Wood et al. (1985).

The finding charts in red are presented for each variable in Fig. 8. They correspond to the epoch for which the stellar magnitude and blending has been studied (JD=2448678.3). Each chart is labelled with the name of the variable. A cross indicates the position at which the variable star has been detected.

8. Conclusion

Besides being a by-product of the microlensing searches, the variable stars constitute their background and their understanding and discrimination are important (e.g. della Valle & Livio (1996)). They need to be catalogued for any on-line microlensing searches (cf. MACHO and EROSII). In this paper, we have produced a comprehensive catalogue of 631 variable stars selected over a 0.25 deg² field in the LMC Bar with the Pixel Method applied to a 120-day window, with a sampling of about one measurement per day. For each variable star, we provide an astrometric position accurate within 1'', together with a finding chart. The study of their position in the CMD shows that this catalogue is dominated by a population of LT&LPV, while a few “bluer” variables have also been detected. Cross-identification with existing catalogues shows that 11 % of them have already been studied elsewhere. We hence enlarge by a factor of 10 the number of LT&LPV detected in this area of the LMC Bar.

The pixel analysis presented here allows a selection of variable objects independently of a photometry. It hence uses all the information present in the frames but does not provide a photometry for these objects. It is complementary to the image subtraction techniques. We have shown that not surprisingly the pixel light curves are significantly polluted by blending, especially in blue and that their conversion in magnitude can only be rough. Hence, for each variable star, we provide an indicator of blending in both colours. The preliminary study of these variable stars together with their cross-identification with previous works show that our photometry does not introduce significant bias on the overall distribution. Recent improvements of the image subtraction techniques developed for microlensing searches (Alard 1999, Alcock et al. 1999a,b) will have to be considered for the future to improve the photometry of the variable stars detected in such crowded fields (e.g. Olech et al. 1999). However, most of these objects are Long Period Variables better characterized with IR photometry than optical non-standard photometry anyway.

The limitation of this dataset is hence reached and it needs to be complemented by other data. In a companion paper, we will extend these selected light curves to the whole EROS I baseline (850 days window), with the 1992-94 data taken with a different set of filters. This will enable us to study the periodicity of these variable stars. In a forthcoming paper, we will cross-identify these variable stars with the IJK photometry of the DENIS catalogue.

Table 2. Catalogue of the variable objects detected in this paper. They are sorted in order of increasing right ascension. It can be retrieved at <http://cdsweb.u-strasbg.fr/htbin/Cat?J/A%2bAS/145/11>.

Fig.8. 1.2' × 1.2' finding charts for each variable in the R_{EROS} filter. It is available in the paper version of the article at A&AS or electronically at <http://www.edpsciences.com/articles/astro/full-2000/13/ds9463/node10.html>.

Acknowledgements. We thank the EROS collaboration (<http://www.lal.in2p3.fr/recherche/eros/erosa.html>) for giving us their 91-92 data, and Marc Moniez for a careful reading of this manuscript. The U plate used for the astrometry was taken at the ESO Schmidt telescope at La Silla. We thank the MAMA team for scanning and reducing this plate. We acknowledge Dave Monet for the informations he kindly provided on the PMM/USNO catalogue. We are particularly grateful to C. Lamy for her useful help on data handling during this work, done in part on the computers of PCC-Collège de France. A.-L. Melchior has been supported by a European contract ERBFMBICT972375 at QMW. This research has made use of the NASA/IPAC Extragalactic Database (NED) which is operated by the Jet Propulsion Laboratory, California Institute of Technology, under contract with the National Aeronautics and Space Administration. The VizieR service (Ochsenbein, 1997) at CDS has been used throughout this work.

References

- Alard, C., 1999, astro-ph/9903111
- Alard, C., Guibert, J., 1997, A&A 326, 1
- Alard, C., Lupton, R. H., 1998, ApJ 503, 325
- Alcock, C., et al. 1997a, ApJ 486, 697
- Alcock, C., et al., 1997b, ApJ 491, L11
- Alcock, C., et al., 1997c, ApJ 479, 119
- Alcock, C., et al., 1999a, ApJ 521, 602
- Alcock, C., et al., 1999b, ApJS 124, 171
- Ansari, R., et al., 1997, A&A 324, 843
- Ansari, R., et al., 1999, A&A 344, L49
- Arnaud, M., et al., 1994, Exp. Astron. 4, 265
- Arnaud, M., et al., 1994, Exp. Astron. 4, 279
- Artiukhina, N., et al. (eds.), 1995, General Catalogue of Variable Stars, 4rd ed., vol.V. Extragalactic Variable Stars, Kosmosinform, Moscow
- Aubourg, E., et al., 1995, A&A 301, 1
- Baillon, P., et al., 1993, A&A 277, 1
- Beaulieu, J.-Ph., et al., 1995, A&A 303, 137
- Beaulieu, J.-Ph., et al., 1996, Sci 272, 995
- Bertelli, G. et al., 1994, A&AS 106, 275
- Bertin, E., Arnouts, S., 1996, A&A 117, 393
- Cardelli, C. et al., 1989, ApJ 345, 245
- Crotts, A., Tomaney, A., 1996, ApJ 473, L87
- della Valle, M., Livio, M., 1996, ApJ 457, L77
- Dickel, H., et al., 1987, A&AS 68, 75
- Grisson, Ph., 1994, Ph.D. thesis, Université de Paris VII, Paris
- Grisson, Ph., et al., 1995, A&AS 109, 447
- Haberl, F., Pietsch, W., 1999, A&A 344, 521

- Hill, V., Beaulieu, J.-Ph., 1997, p:267 Variables Stars and the Astrophysical Returns of the Microlensing Surveys. ed. by R. Ferlet, J.-P. Maillard and B. Raban.
- Hughes, S., 1989, AJ 97, 1634
- Hughes, S., Wood, P. 1990, AJ 99, 784
- Kroupa, P., Bastian, U., 1997, in ESA Symposium 402 'Hipparcos - Venice '97', p:615, B. Battrick, M.A.C. Perryman & P.L. Bernacca (eds)
- Marx, M., et al., 1997, A&AS 126, 325
- Melchior, A.-L. et al., 1998, A&A 339, 658
- Melchior, A.-L. et al., 1999, A&AS 134, 377
- Ochsenbein, F., 1997, Baltic Astronomy 6, 221
- Olech, A. et al., 1999, MNRAS 310, 759
- Palanque-Delabrouille, N. et al., 1998, A&A 332, 1
- Queinnec, F., 1994, Ph.D. thesis, Université de Paris VII, Paris
- Renault, C., 1996, Ph.D. thesis, Université de Paris VII, Paris
- Renault, C., et al., 1997, A&A 324, L69
- Robichon, N., et al., 1995, A&A 304, 132
- Schwering, P., Israel, F., 1991, A&A 246, 231
- Stetson, P. B., 1987, PASP 99, 191
- Tomaney, A. B., Crotts, A., 1996, AJ 112, 2872
- Udalski, A., et al., 1994, Acta Astron. 44, 165
- Wood, P., et al., 1985, ApJ 290, 477

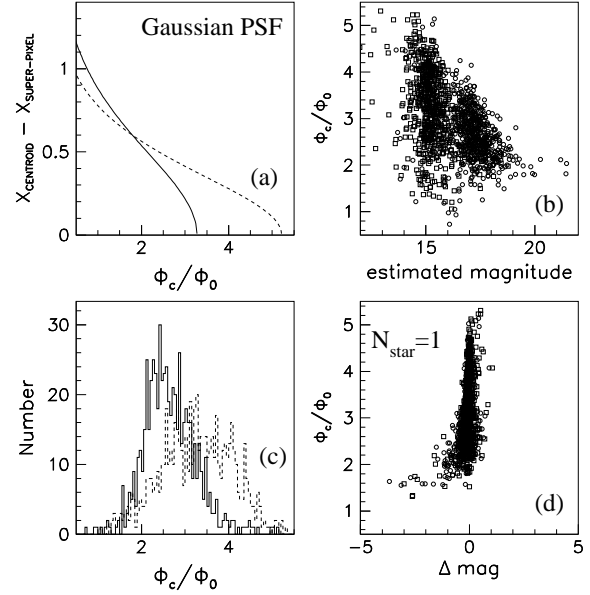


Fig. A.1. Quantification of blending. Square symbols correspond to red measurements and circle to blue. **a)** The position of the star's centroid as a function of the ϕ_c/ϕ_0 ratio is displayed for a single Gaussian PSF (seeing=2.0-1.6 arcsec), without any crowding. In addition, cylindrical symmetry is assumed. **b)** The measured ratio ϕ_c/ϕ_0 , which also includes a measure of the S/N ratio, shows a strong correlation with the magnitude of the stars at JD=2448678.3. **c)** Histograms of the measured ϕ_c/ϕ_0 ratio in blue (full line) and in red (dashed line) of all the selected light curves: blending is stronger in blue **d)** Dependence of the ratio ϕ_c/ϕ_0 as a function of the difference between the estimated magnitude and the magnitude of the closest star detected by DAOPHOT at the epoch JD=2448678.3 for $N_{\text{star}} = 1$, discussed above and in Fig. A.2b.

Appendix A: Limitations of the Pixel Method

Figure A.1 displays the behaviour of the ratio ϕ_c/ϕ_0 computed for the variable stars of the catalogue. Figure A.2 compares our magnitude estimate with the DAOPHOT one for the selected light curves.

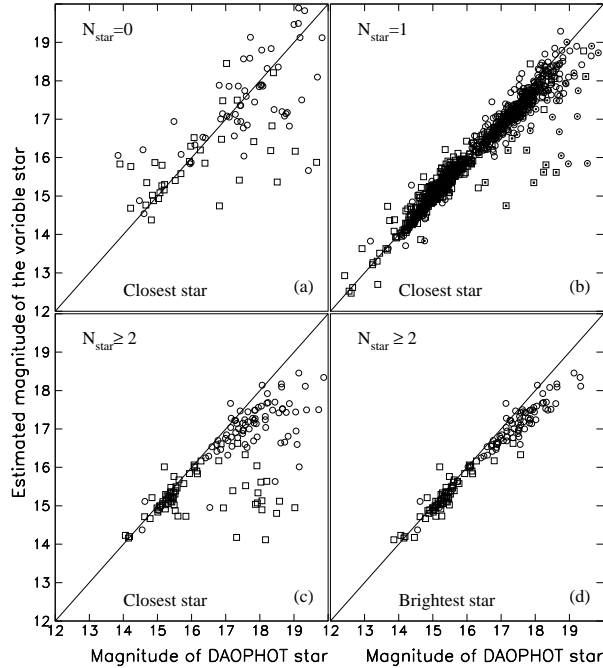


Fig. A.2. Study of the crowding conditions of each variable star of the catalogue with magnitude estimates at the epoch $JD=2448678.3$. The squares correspond to the red measurements and the circles to the blue ones. Each panel corresponds to a given value of N_{star} , the number of stars in the super-pixel, as detected by DAOPHOT. **a)** These points gather stars unresolved at the epoch studied (the majority in blue), stars missed by DAOPHOT (bad PSF or other defect), mis-alignment of the super-pixel with respect to the variable star, and few apparently spurious variations. No correlation is observed with the closest star. **b)** There is a good correlation between the magnitude of the star detected by DAOPHOT and the estimated magnitude, except for a few ones. Filled symbols are measurements for which there is a brighter star within 3 pixels of the centre of the super-pixel, and are clearly affected by blending. The observed dispersion, and in particular the points for which the DAOPHOT magnitude is brighter, is mainly due to the fact that the precision on the position of the centre of the super-pixel is 1 pixel, whereas the position of the centroid of the star defined by DAOPHOT is much more accurate. Panel **c)** displays the correspondence between the estimated magnitude and the magnitude of the *closest* star detected by DAOPHOT. A significant component of blending can be observed. Panel **d)** shows a better correlation as the *brightest* star detected by DAOPHOT in the super-pixel has been used. At the dim end, the crowding limit produces unavoidable blending.

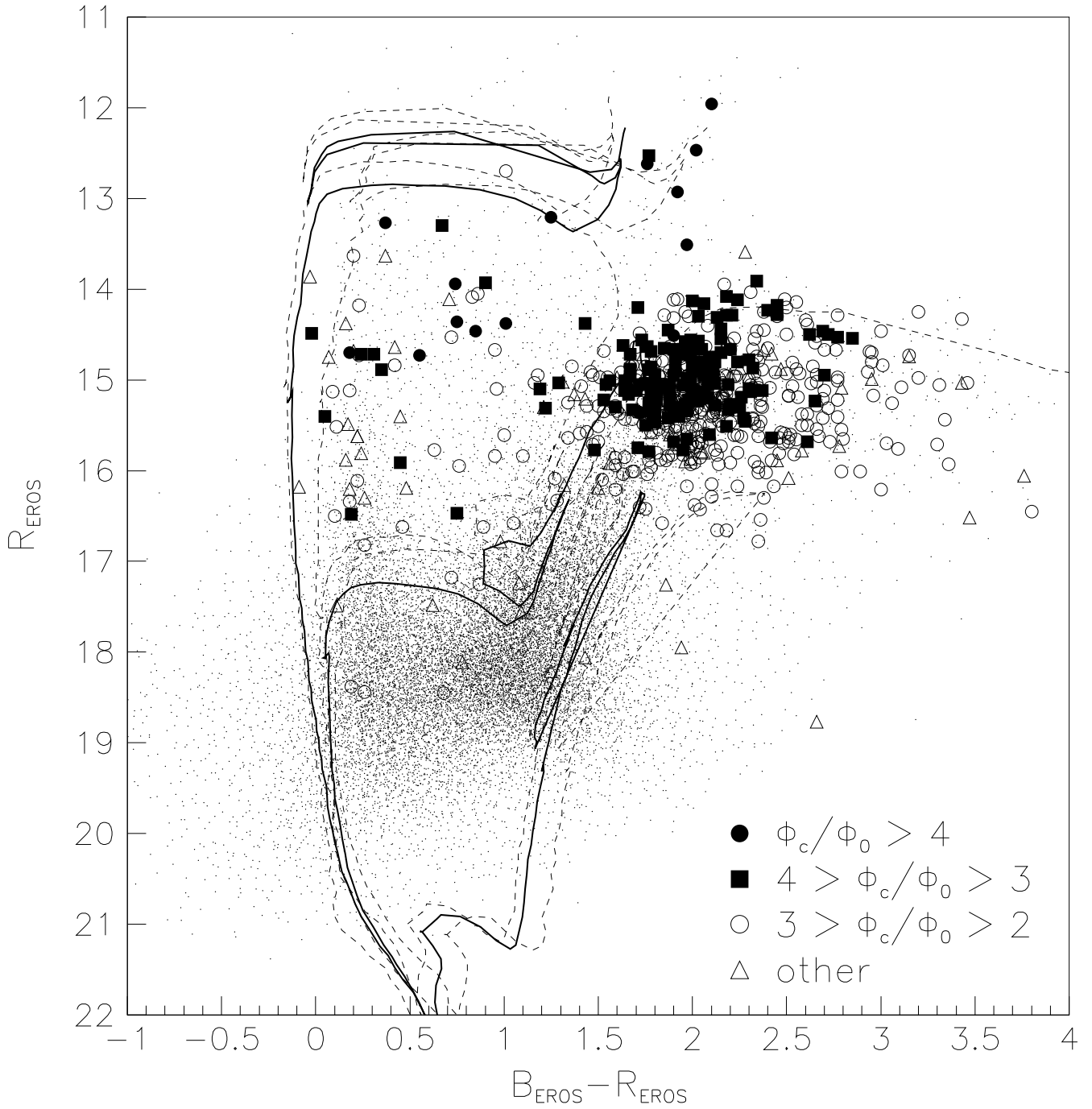


Fig. 4. CMD at JD=2448678.3: small dots correspond to the stars detected with DAOPHOT, symbols to the 631 selected variations. The different symbols correspond to different ranges of the ϕ_c/ϕ_0 ratio : filled symbols correspond to stars with a high S/N ratio and not affected by crowding. The superimposed isochrones (full lines) are adapted from Bertelli et al. (1994) to the EROS system (Grison et al. 1995) with a foreground extinction $A_{B_{\text{EROS}}} = 0.54$ and $A_{R_{\text{EROS}}} = 0.37$, deduced from reddening $E(B-V)=0.15$ measured by Schwering & Israel (1991) with the extinction law from Cardelli et al. (1989). They correspond to LMC metallicity ($Z = 0.008$), helium abundance ($Y = 0.25$) with ages of $\log(\text{age})=7.4, 8.4$ and 9.4 . The dashed lines show the uncertainties introduced on each isochrone by the photometric transformation.